ChemElectroChem

Research Article
doi.org/10.1002/celc.202200210

Chemistry Europe
European Chemical Societies Publishing

www.chemelectrochem.org

Special Collection

Gas-Phase Errors Affect DFT-Based Electrocatalysis Models of Oxygen Reduction to Hydrogen Peroxide

Michell O. Almeida+,[a, b] Manuel J. Kolb+,[a] Marcos R. V. Lanza,[b] Francesc Illas,*[a] and Federico Calle-Vallejo*[a]

Electrochemical production of H_2O_2 is more benign and affordable than the conventional route, yet its adoption requires the discovery of robust, cost-effective catalysts. DFT-based models lead to conspicuous breakthroughs but had some known limitations, for instance the poor description of molecules with certain chemical bonds. Here, the errors in H_2O_2 and O_2 displayed by various GGAs, meta-GGAs and hybrids were assessed and semi empirically corrected. The errors in O_2 with respect to experiments were in the range of -0.95 to -0.22 eV, whereas those in H_2O_2 spanned from -0.53 to -0.04 eV. Thus, single and double O—O bonds were poorly described in general, and the errors were nearly twice as negative for double bonds. Furthermore, these errors introduced large deviations in the predictions of free energies for O_2 reduction to H_2O_2, and the equilibrium potentials and optimal adsorption energies of *OOH could either be sizably overestimated or underestimated.

Introduction

Although clean and safe drinking water is essential for human health, developing countries still face great challenges in their efforts to provide it for their citizens. In fact, contamination by microorganisms and chemicals such as endocrine disruptors pose a significant risk to humans and ecosystems.[1,2] Endocrine disruptors are substances that bind to hormone receptors and can negatively affect their normal functionality. They are classified as persistent organic pollutants and might be harmful even at low concentrations in the scales of parts per billion or trillion. The removal of these pollutants in water treatment plants is difficult, which calls for new technologies to detect and degrade these chemicals.[3–6]

Numerous approaches are currently investigated to treat wastewater, one of them being oxidative processes. These use reactive species such as the hydroxyl radical (•OH) to degrade water pollutants and are often derived from hydrogen peroxide

(H_2O_2). This commodity chemical is mostly produced at large-scale chemical plants by means of the energy-intensive and waste-producing anthraquinone process.[7] An alternative, decentralized and smaller-scale way of producing H_2O_2 is by the electrochemical oxygen reduction reaction (ORR) through a two-electron route (in acidic media: $O_2 + 2H^+ + 2e^- \leftrightarrow H_2O_2$).[8–10] The 2e− ORR competes with the more extensively investigated 4-electron ORR to H_2O (in acid: $O_2 + 4H^+ + 4e^- \leftrightarrow 2H_2O$).[11–16]

The selectivity of the 2e− vs. 4e− ORR is supposedly governed by the stability of a common intermediate, namely *OOH. In other words, the two Sabatier-type activity plots are closely connected. In fact, it is known that active materials for H_2O_2 production such as Co porphyrins and Au lie on the weak-binding (right) leg of the 4e− ORR volcano.[17–19] The two Sabatier-type volcanoes can be built in terms of the adsorption energy of *OH (ΔG_{OH}), which is the prototypical 4e− ORR intermediate and is connected to that of *OOH (ΔG_{OOH}) via a simple and persistent linear scaling relation.[20–24] A widely accepted reaction pathway for the 2e− ORR mediated by *OOH is described in Equations (1) and (2).

$$* + O_2 + H^+ + e^- \leftrightarrow {}^*OOH \tag{1}$$

$$^*OOH + H^+ + e^- \leftrightarrow H_2O_2 + {}^* \tag{2}$$
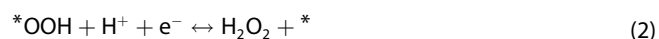
We note that other mechanisms are possible that involve chemical steps such as O_2 dissociation to produce 2*O and the coupling of 2*OH to produce H_2O_2, but the kinetics of such chemical steps is usually less favorable than the corresponding electrochemical steps in Equations (1) and (2), in particular as the overpotential increases (see also the Computational methods section).[25–27] According to Equations (1) and (2), the potential-limiting step for the two-electron reduction of O_2 toward H_2O_2 is either the surface formation of *OOH or its subsequent hydrogenation.

[a] Dr. M. O. Almeida,+ Dr. M. J. Kolb,+ Prof. F. Illas, Dr. F. Calle-Vallejo
Department of Materials Science and Chemical Physics & Institute of Theoretical and Computational Chemistry (IQTCUB)
University of Barcelona
Martí i Franquès 1,08028 Barcelona, Spain
E-mail: francesc.illas@ub.edu
        f.calle.vallejo@ub.edu
[b] Dr. M. O. Almeida,+ Prof. M. R. V. Lanza
São Carlos Institute of Chemistry
University of São Paulo
Avenida Trabalhador São Carlense, Parque Arnold Schimidt, São Carlos 13566-590, Brazil
[+] These authors contributed equally to this work.

ChemElectroChem

Research Article
doi.org/10.1002/celc.202200210

**Chemistry
Europe**

European Chemical
Societies Publishing

To computationally evaluate the catalytic performance and selectivity of electrocatalysts for this reaction, density functional theory (DFT) calculations making use of the generalized gradient approximation (GGA) are often used in conjunction with the computational hydrogen electrode approach.[14,25,26] GGA functionals are widely used in computational analysis of metals in view of the good correlation with experimental values for bulk and surface properties.[28,29] However, it is known that the gas-phase energetics at the GGA level do not always match the experimental values, in particular when the molecules have multiple bonds,[14,25,26,30] as is the case of O_2. This is because DFT has problems describing the exchange contribution to the energy of molecules with strong static correlation effects, such as first-row molecules with several interacting electron pairs. The errors are partially compensated by the contribution of the correlation energy and become smaller as one moves from LDA to GGA functionals and beyond to meta-GGA and hybrid functionals.

The so-called meta-GGA functionals are a more recent approach including the electron density, the density gradient, and an approximation to the kinetic energy density, which show improved results for describing covalent bonds and metallic bonds.[31,32] Lastly, hybrid functionals, which include exact, non-local Fock exchange, are computationally expensive, especially when using plane-wave basis sets, but show improved energetic accuracy for molecular systems.[33]

Despite the large differences in computational cost and concomitant accuracy, the DFT description of O_2 and other molecules with multiple bonds is generally poor. In addition, hybrid functionals ought not to be used on metals in view of the delocalized nature of their electronic structure. In fact, the error of hybrid functionals for properties of bulk metals is significantly larger than those of GGA functionals.[28] This poses a fundamental problem for the study with hybrid functionals of interfacial gas-metal phenomena, namely, adsorption and desorption. Thus, semiempirical corrections to GGAs and meta-GGAs provide a swift and accurate compromise to address gas-phase errors for (electro)catalytic processes on metal surfaces,[34–37] which typically proceed as a series of adsorption, recombination, and desorption steps at surfaces.

In this work, we assess the gas-phase errors of H_2O_2 and O_2 for a wide variety of exchange-correlation functionals across three levels of theory (GGAs with and without incorporating nonlocal interactions, meta-GGAs, hybrids). We find that the errors are generally large and have a noticeable effect in the modelling of the $2e^-$ ORR.

Experimental Section

Computational methods

DFT calculations

We performed DFT calculations for H_2, O_2, H_2O, and H_2O_2 using the VASP code[38] and several GGA (PBE,[39] PW91,[40] RPBE,[41] BEEF,[42] BEEF-vdW,[42] PBE-D2,[39,43] PBE-D3,[39,44] PBE-D3 with Becke-Johnson damping (PBE-D3-BJ),[39,45] vdW-DF,[46,47] and vdW-DF2[48]), meta-GGA

(TPSS[32] and SCAN[31]) and hybrid functionals (HSE06,[49] B3LYP,[50,51] and PBE0[52]). All molecules were relaxed using the conjugate gradient algorithm until all forces were below 0.01 eV/Å. The atomic cores were represented using the projector augmented-wave (PAW) method[53] and Gaussian smearing was used with an electronic temperature of 0.001 eV to ease the convergence of the self-consistent process, after which all energies were extrapolated to 0 K. For all molecules, the unit cell chosen was a cube with a side of 15 Å and, accordingly, the k-point sampling included only the Γ-point. For O_2, spin-unrestricted calculations were carried out to describe its triplet ground state. The free energies of the molecules were approximated as: $G = E_{DFT} + ZPE - TS$, where E_{DFT} is the DFT total energy, ZPE is the zero-point energy calculated with DFT within the harmonic oscillator approximation, and the TS values were taken from thermodynamic tables at 298.15 K (see Table S4).[54] We note that the experimental ZPEs of H_2, O_2, H_2O and H_2O_2 are 0.27, 0.10, 0.56 and 0.69 eV.[55] The averages of the calculated ZPEs in Table S2 are 0.28 ± 0.01, 0.10 ± 0.00, 0.58 ± 0.01, 0.70 ± 0.02 eV, respectively. Thus, we conclude that ZPEs are not a major source of discrepancy between experiments and calculations. Moreover, we did not incorporate heat capacity effects in our modelling because recent works showed that heats of formation are not substantially modified by them from 0 to 298.15 K.[56]

To ascertain the convergence of the calculations with respect to the plane-wave cutoff, we calculated with PW91 the formation free energy of $H_2O_{2(g)}$ [i.e., $O_{2(g)} + H_{2(g)} \leftrightarrow H_2O_{2(g)}$] and that of two H_2O molecules [i.e., $O_{2(g)} + 2H_{2(g)} \leftrightarrow 2H_2O_{(g)}$] with a cutoff energy in the range of 350–1000 eV in steps of 50 eV. Convergence within ± 0.05 eV for PW91 and TPSS is found at 450 eV, as shown in Figures 1 and S1 (see also Tables S1, S2, S7 and S8). Thus, this plane-wave cutoff, common in computational (electro)catalysis, was used for the other functionals.

Two-electron ORR modelling

In experiments, the standard free energy of formation of aqueous H_2O_2 is -1.36 eV.[57] Since the corresponding value in the gas phase is -1.09 eV, we conclude that the solvation energy of hydrogen peroxide in water is -0.27 eV. Thus, we added -0.27 eV to the calculated free energy of formation of $H_2O_{2(g)}$ to approximate that of $H_2O_{2(aq)}$.

The standard equilibrium potential of the $2e^-$ ORR (in V vs RHE) can be computed from the reaction free energy (in eV) as: $U^0_{2e^--ORR} = -\Delta_f G^0_{H_2O_2(aq)}/2e^-$. In this order of ideas, the free energies at 0 V vs RHE of Equations (1) and (2) are, respectively: $\Delta G_1 = \Delta G_{OOH}$ and $\Delta G_2 = \Delta_f G^0_{H_2O_2(aq)} - \Delta G_{OOH}$. Furthermore, the adsorption energy of *OOH of the ideal catalyst is: $\Delta G_{OOH,ideal} = \Delta_f G^0_{H_2O_2(aq)}/2$. This energy guarantees that the thermodynamic overpotential ($\eta_{ORR,2e^-} = U^0_{2e^--ORR} + \max(\Delta G_1, \Delta G_2)/e^-$) is zero for the hypothetical ideal catalyst.

Furthermore, chemical steps on the ideal catalyst should have null free energy changes.[26] Thus, the dissociative adsorption of O_2 ($O_2 + 2^* \rightarrow 2^*O$) on the ideal catalyst should have $\Delta G_{diss} = 0$. A previously reported Brønsted-Evans-Polanyi (BEP) relation for O_2 dissociation is:[58] $G_{TS} \approx 0.58\Delta G_{diss} + 1.11$. If the ideal catalyst follows such BEP relation, its barrier would be $G_{TS} \approx 1.11 \pm 0.26$ eV, which is above the limit for surmountable barriers at 298.15 K set at 0.75 eV[59] to obtain turnover frequencies of at least 1 s^{-1} per site. In addition, electrochemical barriers tend to be smaller and decrease as the overpotential is increased. For instance, O_2 hydrogenation to give *OOH has a barrier of 0.37 eV on Pt(111) at 0.9 V vs RHE.[27] At a typical potential of the $2e^-$ ORR, let us say 0.5 V vs RHE, that barrier will be around 0.2 eV, assuming a symmetry factor of 0.5. All this suggests that it is more likely for active catalysts for H_2O_2
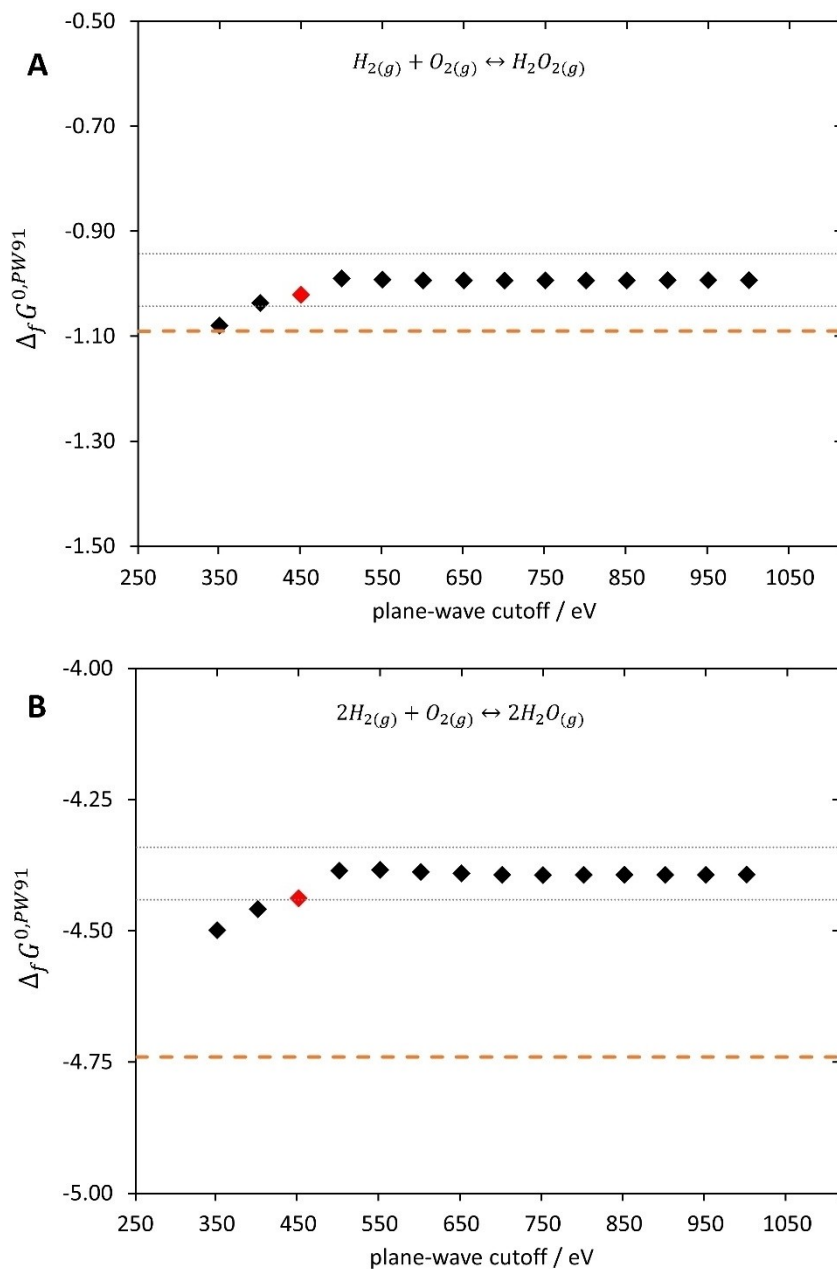
ChemElectroChem

Research Article
doi.org/10.1002/celc.202200210

Chemistry
Europe
European Chemical
Societies Publishing

Figure 1. Plane-wave cutoff convergence test for PW91 in the range 350–1000 eV for the standard formation energy of H_2O_2 (A) and 2 H_2O molecules (B) in the gas phase. The values at 450 eV appear in red and the experimental values correspond to the orange dashed lines. The gray dashed lines are located at ± 0.05 eV of the average free energy of the plateau (500–1000 eV). See further details in sections S1 and S4.

production to hydrogenate O_2 instead of dissociating it. Hence, we only considered here the pathway in Equations (1) and (2) for the ideal catalyst.

Results and Discussion

Gas-phase errors

The DFT error for a given molecule i (ε_i) is defined with respect to the experiments as shown in Eq. (3).[34]

$$\varepsilon_i = \Delta_f G_i^{0,\,\text{DFT}} - \Delta_f G_i^{0,\text{exp}} \tag{3}$$

For gas-phase hydrogen peroxide we have: $\Delta_f G_{H_2O_{2(g)}}^{0,\text{exp}} = -1.09$ eV. Furthermore, given that H_2 and H_2O only have H–H and O–H single bonds, they are generally well described by most functionals.[30,60] Thus, in the DFT-calculated formation energy of $H_2O_{2(g)}$ the total error (ε_T) is a convolution of those of O_2 and $H_2O_{2(g)}$. In fact, starting from Equation (3), it can be shown that the total error can be expressed as in Eq. (4).

$$\varepsilon_T = \varepsilon_{H_2O_2} - \varepsilon_{O_2} \tag{4}$$

ChemElectroChem

Research Article
doi.org/10.1002/celc.202200210

**Chemistry
Europe**
European Chemical
Societies Publishing

To isolate the H_2O_2 errors, we first assessed those of O_2 based on the formation of gas-phase water ($\frac{1}{2}O_{2(g)} + H_{2(g)} \leftrightarrow H_2O_{(g)}$, $\Delta_f G^{0,exp}_{H_2O(g)} = -2.37$ eV), in line with previous works.[26] Table 1 contains the errors in $O_{2(g)}$ and $H_2O_{2(g)}$ and their convolution for all functionals under study. As expected,[30] the errors in Table 1 for O_2 are generally rather large, falling in the range of -0.95 to -0.22 eV. Similarly, the errors in H_2O_2 tend to be negative, yet their magnitude is smaller than those of O_2. The last column of Table 1 provides the ratio of the two errors. On average, the ratio is 0.46 ± 0.15, which indicates that the errors in the description of O–O bonds are cumulative. In other words, a single O–O bond is usually described by a given functional with higher accuracy than a double O–O bond, and in both cases the errors are sizable. It is also worth mentioning that the total errors when neither O_2 nor H_2O_2 are corrected [ε_T, see Eq. (4) and Table 1] are significant and tend to be positive as a result of error cancellation.

For O_2, one can organize the functionals in decreasing order of accuracy as: PBE0, HSE06, PW91, B3LYP, SCAN, PBE-D3-BJ, PBE-D3, PBE-D2, PBE, RPBE, BEEF, BEEF-vdW, TPSS, vdW-DF2 and vdW-DF, where PBE0 is the most accurate. For H_2O_2, the order of accuracy is: PBE0, HSE06, B3LYP, SCAN, PW91, BEEF, PBE, PBE-D3-BJ, PBE-D3, PBE-D2, RPBE, BEEF-vdW, TPSS, vdW-DF, and vdW-DF2. The two orderings are rather similar: as expected, hybrid functionals perform better than the GGA family, being PBE0 the most accurate functional for both O_2 and H_2O_2. One of the meta-GGA functionals (SCAN) has intermediate accuracy between hybrid and GGA functionals, while the other one (TPSS) performs poorly. For both O_2 and H_2O_2, the largest errors are found for vdW functionals.

To close this section, we note that the errors in H_2O_2 were calculated previously for a few GGA functionals with and without nonlocal interactions.[23] Those errors, which were calculated on the basis of a different reaction ($2H_2O_{(g)} \leftrightarrow H_{2(g)} + H_2O_{2(g)}$) and methodology appear in parenthesis in Table 1. In general, there is good agreement between the present and previous results, which supports the conclusion that the DFT description of the O–O bond in H_2O_2 is not good enough. Furthermore, our results show that the errors are present in most functionals, even those in higher levels of

theory, such as meta-GGAs and hybrids. We note in passing that the work of Christensen et al. has also indicated that the errors in the O–O bonds displayed by H_2O_2 might be present in *OOH.[23]

Oxygen reduction to hydrogen peroxide

Once substantial gas-phase errors were pinpointed and corrected semiempirically, we set out to investigate their effect on the $2e^-$ ORR. According to Equation (1), the energetics of the first step of the reaction is affected by the error in O_2. Moreover, according to Equation (2), the second step is affected by the error in H_2O_2. The equilibrium potentials are computed as described in the Computational methods section and appear in Table 2 (the free energies of formation can be found in Tables S5 and S6).

As a first approximation, we will restrict the electrocatalysis modelling to the free-energy diagrams of the thermodynamically ideal catalyst. Such a hypothetical catalyst is "electrochemically symmetric", namely, all electrochemical steps are energetically identical.[24,61,62] In other words, the formation of *OOH [Eq. (1)] requires as much energy as its hydrogenation [Eq. (2)]. Anticipating the catalytic behavior of this theoretical catalyst is useful to know the thermodynamic best-case scenario and, therefore, establish realistic expectations for the performance of actual catalysts.

Figure 2 shows the free-energy diagrams of the ideal catalyst for the $2e^-$ ORR when neither the errors in O_2 nor in H_2O_2 are corrected (see the calculated values of $U^{0, NC}_{ORR,2e^-}$ in Table 2) and includes the data for the ideal experimental catalyst. Because the total errors are generally positive [ε_T, see Eq. (4) and Table 1], the calculated equilibrium potentials are less positive than the experimental one. This means that fully uncorrected functionals predict smaller free energies than the experimental one for the $2e^-$ ORR, as a result of the convolution of errors in O_2 and H_2O_2.

On the other hand, Figure 3 shows that if only O_2 is corrected, the predicted equilibrium potentials are larger than in experiments. This indicates that O_2-corrected DFT results

Table 1. Errors (in eV) with respect to experiments of various exchange-correlation functionals in describing O_2 and H_2O_2. ε_T is the error associated with the formation of gas-phase H_2O_2 when neither O_2 nor H_2O_2 are corrected. The values in parenthesis are from Ref. [23].

xc-functional family	xc-functional	$\varepsilon_T = \varepsilon_{H_2O_2} - \varepsilon_{O_2}$	ε_{O_2}	$\varepsilon_{H_2O_2}$	$\varepsilon_{H_2O_2}/\varepsilon_{O_2}$
GGA	PBE[39]	0.22	−0.48	−0.26 (−0.25)	0.54
	PW91[40]	0.07	−0.30	−0.23	0.76
	RPBE[41]	0.46	−0.75	−0.29 (−0.29)	0.39
	BEEF[42]	0.57	−0.81	−0.25	0.30
GGA-vdW	BEEF-vdW[42]	0.49	−0.83	−0.34 (−0.26)	0.41
	PBE-D2[39,43]	0.21	−0.48	−0.27	0.56
	PBE-D3[39,44]	0.21	−0.48	−0.27	0.55
	PBE-D3-BJ[39,44,45]	0.20	−0.46	−0.27	0.58
	vdW-DF[46,47]	0.46	−0.95	−0.49 (−0.41)	0.51
	vdW-DF2[48]	0.38	−0.91	−0.53 (−0.44)	0.58
Meta-GGA	TPSS[32]	0.45	−0.91	−0.46	0.51
	SCAN[31]	0.27	−0.46	−0.19	0.42
Hybrid	HSE06[49]	0.16	−0.22	−0.05	0.24
	B3LYP[50,51]	0.24	−0.36	−0.12	0.34
	PBE0[52]	0.18	−0.22	−0.04	0.18

ChemElectroChem

Research Article
doi.org/10.1002/celc.202200210

**Chemistry
Europe**
European Chemical
Societies Publishing

Table 2. Standard equilibrium potential (in V vs RHE) of the 2e⁻ ORR for various exchange-correlation functionals. The experimental value is provided for comparison, which can be found in the literature or from DFT by simultaneously correcting O_2 and H_2O_2 with the values in Table 1. *NC*: No gas-phase corrections applied. *OC*: gas-phase corrections applied only to O_2.

xc-functional family	xc-functional	$U^{0, NC}_{2e^- ORR}$	$U^{0, OC}_{2e^- ORR}$
GGA	PBE[39]	0.57	0.81
	PW91[40]	0.65	0.80
	RPBE[41]	0.45	0.83
	BEEF[42]	0.40	0.81
GGA-vdW	BEEF-vdW[42]	0.44	0.85
	PBE-D2[39,43]	0.58	0.82
	PBE-D3[39,44]	0.58	0.82
	PBE-D3-BJ[39,44,45]	0.58	0.82
	vdW-DF[46,47]	0.45	0.93
	vdW-DF2[48]	0.49	0.95
Meta-GGA	TPSS[32]	0.46	0.91
	SCAN[31]	0.55	0.78
Hybrid	HSE06[49]	0.60	0.71
	B3LYP[50,51]	0.56	0.74
	PBE0[52]	0.59	0.70
Experimental		0.68	0.68

overestimate the magnitude of the 2e⁻ ORR reaction energy. Analyzing Figures 2 and 3 together with Table 2, we note that the equilibrium potentials and ideal *OOH adsorption energies change drastically depending on the functional because of gas-phase errors and only when H_2O_2 and O_2 are simultaneously corrected can computational predictions match the experimental results. Although some values in Table 2 are close to experiments (in particular for hybrid functionals), it is dangerous to rely on error cancellation. Interestingly, depending on the degree of correctness of the gas-phase, the equilibrium potentials are either appreciably underestimated or overestimated. The same can be said about the optimal values of

ΔG_{OOH}: while ideally it is −0.68 eV, for a widely used functional such as RPBE it is −0.45 and −0.83 eV when no gas-phase corrections are applied and when only O_2 is corrected, respectively. We note, however, that this is not a particularity of RPBE, and all families of functionals in Table 2 behave similarly.

To close the discussion, it is important to note that a common practice in computational electrocatalysis models of the 4e⁻ ORR consists of using experimental values for the reaction energy instead of those calculated with DFT.[14,25,26] That serves the purpose of mitigating the gas-phase error of O_2 because H_2 and H_2O are generally well described. However, such an ad hoc procedure may not work for reactions in which more than one substance has associated gas-phase errors. For instance, that is the case for the electrochemical reduction of CO_2 to CO (where both CO_2 and CO display large gas-phase errors)[34,36,37] and reactions within the nitrogen cycle.[35,63] For the 2e⁻ ORR, as shown in Figures 2–3, such a procedure impedes discerning the O_2 errors from those of H_2O_2, which are convoluted as shown in Equation (4).

Conclusions

For a number of environmental, industrial, and public health reasons, it is highly desirable to enable the small-scale, decentralized production of hydrogen peroxide. An alternative to do so is the two-electron oxygen reduction reaction. While computational models based on DFT calculations can be a great help when seeking new catalysts for this reaction, gas-phase errors in O_2 and H_2O_2 might limit their predictive power. In this article, we showed that the poor description of O—O bonds, be them single or double, is a general feature of exchange-correlation functionals at the GGA, meta-GGA and hybrid levels
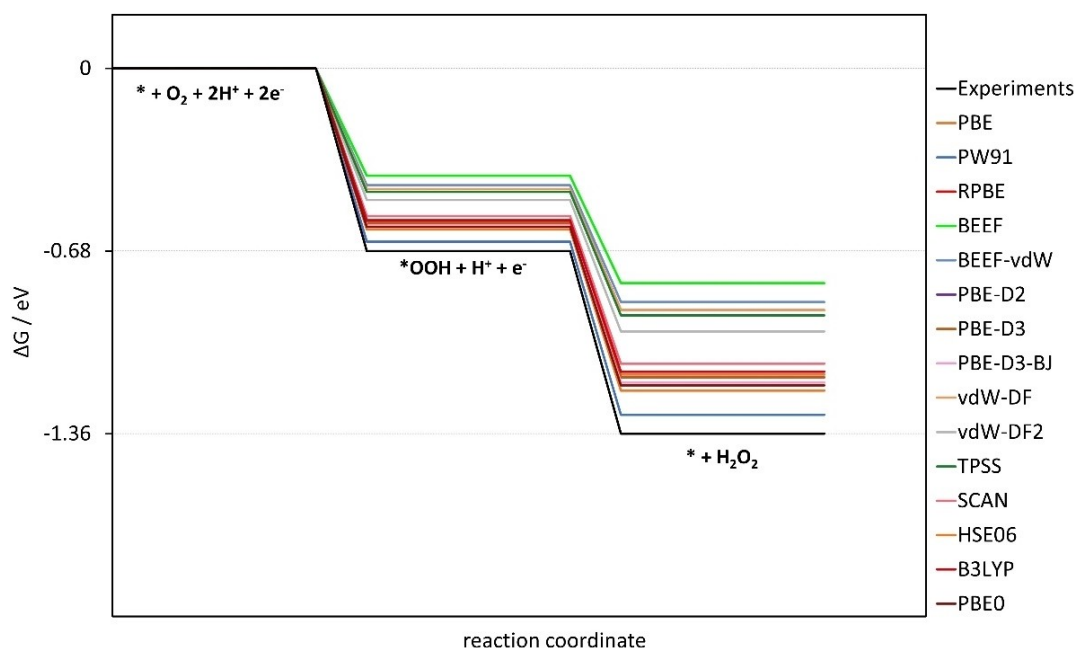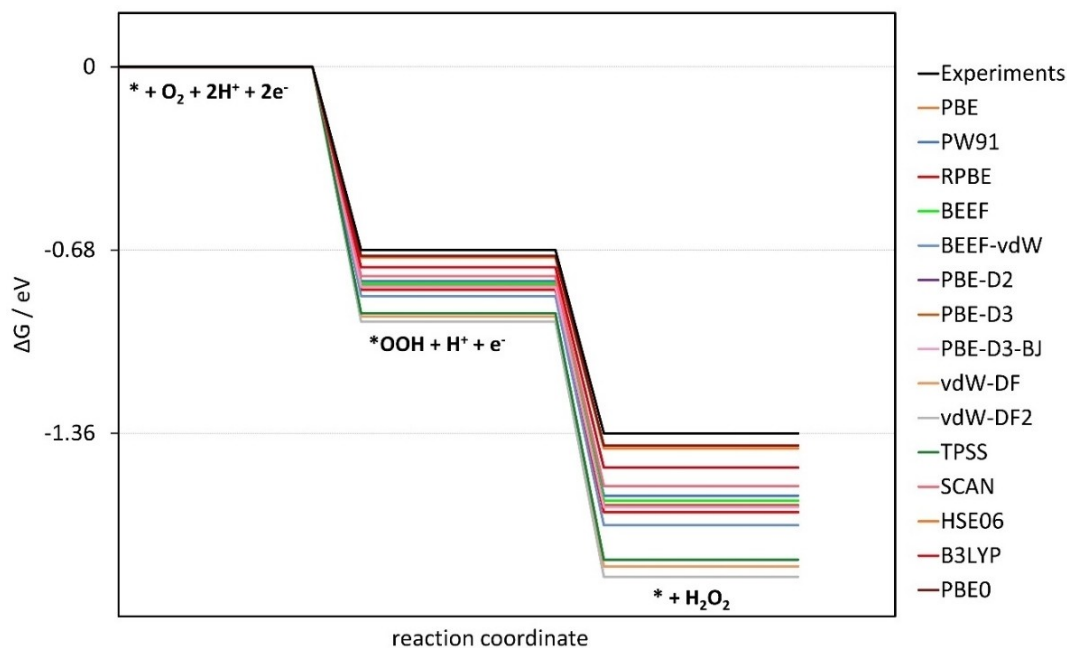

Figure 2. Free-energy diagram at 0 V vs RHE for the optimal catalyst of the two-electron ORR using experimental data (black) and DFT calculations without gas-phase corrections. When corrections for O_2 and H_2O_2 are used, the experimental profile is retrieved.

ChemElectroChem

Research Article
doi.org/10.1002/celc.202200210

Chemistry Europe
European Chemical
Societies Publishing

Figure 3. Free-energy diagram at 0 V vs RHE for the optimal catalyst of the two-electron ORR using experimental data (black) and DFT calculations with gas-phase corrections applied only to O_2. When corrections for O_2 and H_2O_2 are used, the experimental profile is retrieved.

of theory. A simple semiempirical scheme based on free energies of formation aided in detecting and correcting such gas-phase errors.

Furthermore, we analyzed the effect of those errors in a computational electrocatalysis model of the $2e^-$ ORR. Depending on the degree of correctness of the free energies of the gases, the equilibrium potentials and optimal adsorption energies of *OOH could either be sizably overestimated or underestimated, such that gas-phase corrections are advisable for both O_2 and H_2O_2. While in this case we focused on the energy profiles of the ideal $2e^-$ ORR catalyst, future studies could focus on the effects over real catalysts.

In the end, we hope that quantitative agreement between experiments and theory regarding the equilibrium potential and associated properties, resulting from a proper description of molecules, becomes an unmissable ingredient in computational electrocatalysis models.

Conflict of Interest

The authors declare no conflict of interest.

Data Availability Statement

The data that support the findings of this study are available in the supplementary material of this article.

[1] A. Gonsioroski, V. E. Mourikes, J. A. Flaws, *Int. J. Mol. Sci.* **2020**, *21*, 1929.
[2] R. P. Schwarzenbach, T. Egli, T. B. Hofstetter, U. von Gunten, B. Wehrli, *Annu. Rev. Environ. Res.* **2010**, *35*, 109–136.
[3] J. Moreira, V. Bocalon Lima, L. Athie Goulart, M. R. V. Lanza, *Appl. Catal. B* **2019**, *248*, 95–107.
[4] M. A. Oturan, J.-J. Aaron, *Crit. Rev. Environ. Sci. Technol.* **2014**, *44*, 2577–2641.
[5] E. R. Kabir, M. S. Rahman, I. Rahman, *Environ. Toxicol. Pharmacol.* **2015**, *40*, 241–258.
[6] T. Deblonde, C. Cossu-Leguille, P. Hartemann, *Int. J. Hyg. Environ. Health* **2011**, *214*, 442–448.
[7] J. M. Campos-Martin, G. Blanco-Brieva, J. L. G. Fierro, *Angew. Chem. Int. Ed.* **2006**, *45*, 6962–6984; *Angew. Chem.* **2006**, *118*, 7116–7139.
[8] A. J. dos Santos, A. S. Fajardo, M. S. Kronka, S. Garcia-Segura, M. R. V. Lanza, *Electrochim. Acta* **2021**, *376*, 138034.

ChemElectroChem

Research Article
doi.org/10.1002/celc.202200210

Chemistry Europe
European Chemical
Societies Publishing

[9] S. Siahrostami, A. Verdaguer-Casadevall, M. Karamad, D. Deiana, P. Malacrida, B. Wickman, M. Escudero-Escribano, E. A. Paoli, R. Frydendal, T. W. Hansen, I. Chorkendorff, I. E. L. Stephens, J. Rossmeisl, *Nat. Mater.* **2013**, *12*, 1137–1143.

[10] K. Jiang, S. Back, A. J. Akey, C. Xia, Y. Hu, W. Liang, D. Schaak, E. Stavitski, J. K. Nørskov, S. Siahrostami, H. Wang, *Nat. Commun.* **2019**, *10*, 3997.

[11] X. Zhao, Y. Liu, *J. Am. Chem. Soc.* **2021**, *143*, 9423–9428.

[12] S. Siahrostami, G. L. Li, V. Viswanathan, J. K. Nørskov, *J. Phys. Chem. Lett.* **2017**, *8*, 1157–1160.

[13] V. Viswanathan, H. A. Hansen, J. K. Nørskov, *J. Phys. Chem. Lett.* **2015**, *6*, 4224–4228.

[14] A. Kulkarni, S. Siahrostami, A. Patel, J. K. Nørskov, *Chem. Rev.* **2018**, *118*, 2302–2312.

[15] C. Zhang, S. Yu, S. Xie, W. Zhang, K. Zheng, N. E. Drewett, S. J. Yoo, Z. Wang, L. Shao, H. Tian, J.-G. Kim, W. Zheng, *Carbon* **2019**, *149*, 370–379.

[16] C. Zhang, W. Zhang, S. Yu, D. Wang, W. Zhang, W. Zheng, M. Wen, H. Tian, K. Huang, S. Feng, J. J. Bentzen, *ChemElectroChem* **2017**, *4*, 1269–1273.

[17] J. H. Zagal, M. T. M. Koper, *Angew. Chem. Int. Ed.* **2016**, *55*, 14510–14521; *Angew. Chem.* **2016**, *128*, 14726–14738.

[18] H. Li, Y. Li, M. T. M. Koper, F. Calle-Vallejo, *J. Am. Chem. Soc.* **2014**, *136*, 15694–15701.

[19] V. Viswanathan, H. A. Hansen, J. Rossmeisl, J. K. Nørskov, *J. Phys. Chem. Lett.* **2012**, *3*, 2948–2951.

[20] I. C. Man, H.-Y. Su, F. Calle-Vallejo, H. A. Hansen, J. I. Martínez, N. G. Inoglu, J. Kitchin, T. F. Jaramillo, J. K. Nørskov, J. Rossmeisl, *ChemCatChem* **2011**, *3*, 1159–1165.

[21] N. Govindarajan, M. T. M. Koper, E. J. Meijer, F. Calle-Vallejo, *ACS Catal.* **2019**, *9*, 4218–4225.

[22] M. T. M. Koper, *J. Electroanal. Chem.* **2011**, *660*, 254–260.

[23] R. Christensen, H. A. Hansen, C. F. Dickens, J. K. Nørskov, T. Vegge, *J. Phys. Chem. C* **2016**, *120*, 24910–24916.

[24] N. Govindarajan, J. M. García-Lastra, E. J. Meijer, F. Calle-Vallejo, *Curr. Opin. Electrochem.* **2018**, *8*, 110–117.

[25] J. K. Nørskov, J. Rossmeisl, A. Logadottir, L. Lindqvist, J. R. Kitchin, T. Bligaard, H. Jónsson, *J. Phys. Chem. B* **2004**, *108*, 17886–17892.

[26] E. Sargeant, A. Illas, P. Rodríguez, F. Calle-Vallejo, *J. Electroanal. Chem.* **2021**, *896*, DOI 10.1016/j.jelechem.2021.115178.

[27] V. Tripković, E. Skúlason, S. Siahrostami, J. K. Nørskov, J. Rossmeisl, *Electrochim. Acta* **2010**, *55*, 7975–7981.

[28] L. Vega, J. Ruvireta, F. Viñes, F. Illas, *J. Chem. Theory Comput.* **2018**, *14*, 395–403.

[29] P. Janthon, S. Luo, S. M. Kozlov, F. Viñes, J. Limtrakul, D. G. Truhlar, F. Illas, *J. Chem. Theory Comput.* **2014**, *10*, 3832–3839.

[30] S. Kurth, J. P. Perdew, P. Blaha, *Int. J. Quantum Chem.* **1999**, *75*, 889–909.

[31] J. Sun, A. Ruzsinszky, J. P. Perdew, *Phys. Rev. Lett.* **2015**, *115*, 36402.

[32] J. Sun, M. Marsman, G. I. Csonka, A. Ruzsinszky, P. Hao, Y.-S. Kim, G. Kresse, J. P. Perdew, *Phys. Rev. B* **2011**, *84*, 35117.

[33] J. Heyd, G. E. Scuseria, M. Ernzerhof, *J. Chem. Phys.* **2003**, *118*, 8207–8215.

[34] L. P. Granda-Marulanda, A. Rendón-Calle, S. Builes, F. Illas, M. T. M. Koper, F. Calle-Vallejo, *ACS Catal.* **2020**, *10*, 6900–6907.

[35] R. Urrego-Ortiz, S. Builes, F. Calle-Vallejo, *ChemCatChem* **2021**, *13*, 2508–2516.

[36] R. Christensen, H. A. Hansen, T. Vegge, *Catal. Sci. Technol.* **2015**, *5*, 4946–4949.

[37] A. A. Peterson, F. Abild-Pedersen, F. Studt, J. Rossmeisl, J. K. Nørskov, *Energy Environ. Sci.* **2010**, *3*, 1311–1315.

[38] G. Kresse, J. Furthmüller, *Phys. Rev. B* **1996**, *54*, 11169–11186.

[39] J. P. Perdew, K. Burke, M. Ernzerhof, *Phys. Rev. Lett.* **1996**, *77*, 3865–3868.

[40] J. P. Perdew, Y. Wang, *Phys. Rev. B* **1992**, *45*, 13244–13249.

[41] B. Hammer, L. B. Hansen, J. K. Nørskov, *Phys. Rev. B* **1999**, *59*, 7413–7421.

[42] J. Wellendorff, K. T. Lundgaard, A. Møgelhøj, V. Petzold, D. D. Landis, J. K. Nørskov, T. Bligaard, K. W. Jacobsen, *Phys. Rev. B* **2012**, *85*, 235149.

[43] S. Grimme, *J. Comput. Chem.* **2006**, *27*, 1787–1799.

[44] S. Grimme, J. Antony, S. Ehrlich, H. Krieg, *J. Chem. Phys.* **2010**, *132*, 154104.

[45] S. Grimme, S. Ehrlich, L. Goerigk, *J. Comput. Chem.* **2011**, *32*, 1456–1465.

[46] M. Dion, H. Rydberg, E. Schröder, D. C. Langreth, B. I. Lundqvist, *Phys. Rev. Lett.* **2004**, *92*, 246401.

[47] G. Román-Pérez, J. M. Soler, *Phys. Rev. Lett.* **2009**, *103*, 96102.

[48] K. Lee, É. D. Murray, L. Kong, B. I. Lundqvist, D. C. Langreth, *Phys. Rev. B* **2010**, *82*, 81101.

[49] A. v. Krukau, O. A. Vydrov, A. F. Izmaylov, G. E. Scuseria, *J. Chem. Phys.* **2006**, *125*, 224106.

[50] A. D. Becke, *J. Chem. Phys.* **1993**, *98*, 5648–5652.

[51] C. Lee, W. Yang, R. G. Parr, *Phys. Rev. B* **1988**, *37*, 785–789.

[52] C. Adamo, V. Barone, *J. Chem. Phys.* **1999**, *110*, 6158–6170.

[53] G. Kresse, D. Joubert, *Phys. Rev. B* **1999**, *59*, 1758–1775.

[54] D. R. Lide, *CRC Handbook of Chemistry and Physics*, CRC Press, **2004**.

[55] NIST Computational Chemistry Comparison and Benchmark Database, NIST Standard Reference Database Number 101, Release 21, August 2020, Editor: Russell D. Johnson III http://cccbdb.nist.gov/ (accessed 2022-02-22).

[56] C. J. Bartel, A. W. Weimer, S. Lany, C. B. Musgrave, A. M. Holder, *npj Comput. Mater.* **2019**, *5*, 4.

[57] Marcel Pourbaix, *Atlas of Electrochemical Equilibria in Aqueous Solutions*, Pergamon Press, Oxford; New York, **1966**.

[58] S. Wang, B. Temel, J. Shen, G. Jones, L. C. Grabow, F. Studt, T. Bligaard, F. Abild-Pedersen, C. H. Christensen, J. K. Nørskov, *Catal. Lett.* **2011**, *141*, 370–373.

[59] S. Nitopi, E. Bertheussen, S. B. Scott, X. Liu, A. K. Engstfeld, S. Horch, B. Seger, I. E. L. Stephens, K. Chan, C. Hahn, J. K. Nørskov, T. F. Jaramillo, I. Chorkendorff, *Chem. Rev.* **2019**, *119*, 7610–7672.

[60] J. Wellendorff, T. L. Silbaugh, D. Garcia-Pintos, J. K. Nørskov, T. Bligaard, F. Studt, C. T. Campbell, *Surf. Sci.* **2015**, *640*, 36–44.

[61] C. H. Kjaergaard, J. Rossmeisl, J. K. Nørskov, *Inorg. Chem.* **2010**, *49*, 3567–3572.

[62] O. Piqué, F. Illas, F. Calle-Vallejo, *Phys. Chem. Chem. Phys.* **2020**, *22*, 6797–6803.

[63] R. Urrego-Ortiz, S. Builes, F. Calle-Vallejo, *ACS Catal.* **2022**, *12 (8)*, 4784–4791.